Rev. Roum. Sci. Techn.– Électrotechn. et Énerg.
Vol. **63**, *1*, pp. 65–70, Bucarest, 2018

ASYMMETRICAL DUTY CYCLE PHASE-SHIFTED DUAL OUTPUT INDUCTION COOKER

AVIJIT CHAKRABORTY[1], PRADIP KUMAR SADHU[2], ARIJIT CHAKRABARTI[3], AMRIK BASAK[4], NITAI PAL[2]

Keywords: Half-bridge inverter, Insulated-gate-bipolar transistor (IGBT), Switching frequency, Power-system-simulator (PSIM), Duty cycle.

This paper presents an analysis of a dual output domestic induction cooker incorporating two half-bridge resonant inverters. The two inverters are subjected to asymmetrical duty cycle phase-shift control strategy to smoothly vary their output powers. This control technique ensures better and more effective performance compared to other conventional control techniques. Both the inverters are connected to two partly magnetically coupled inductive loads sharing a common resonant capacitor. Both the inverters operate with the same switching frequency avoiding inter modulation acoustic noises due to the magnetic coupling between the two loads. The entire system is analyzed and the simulation is accomplished with the help of power system simulator (PSIM) software. The results obtained from the simulation are finally verified with the results obtained from the real time hardware experiment.

1. INTRODUCTION

In modern times, induction heating process has become a very popular method to produce very high and controllable temperature accurately and efficiently [1]. Any induction heating system must consist of at least one high frequency resonant inverter [2]. Different applications need different inverter topologies such as half-bridge inverter [3], full bridge inverters [4, 5] and hybrid inverters [6] respectively. The output power requires to be controlled properly. Different control schemes are so far proposed for power control for wide range and every control scheme has its own advantages and disadvantages. The mostly used fixed frequency control schemes are phase-shift control (PSC) [7], the asymmetrical voltage cancellation control (AVC) [8] and pulse density modulation control schemes (PDM) [9] respectively. Moreover, hybrid control schemes as a mixture of these three schemes can provide better power control. Soft computation techniques like genetic algorithm find successful application for optimum control in Induction heating systems [10].

The rest of the paper is organized as follows. Section 2 describes about the principle of the dual output induction cooker. The two-port network model is analyzed in section 3. Section 4 consists of an analytical approach of asymmetrical duty cycle phase-shift control scheme. Real time hardware experiment is discussed in Section 5. Verification of simulation results with the hardware experimental results are described in the Section 6. Finally, main conclusion is drawn at the end.

2. PRINCIPLE OF DUAL OUTPUT INDUCTION COOKER

In Fig. 1 a dual output half-bridge resonant inverter based induction cooker is shown, which is used in the proposed domestic induction cooking system. It consists of two series resonant loads and both of them share an equivalent resistor *R* and equivalent inductor *L*. Moreover, the dual output induction cooker also shares a resonant capacitor C. The inverter is implemented using four IGBTs (Q_1–Q_4) along with four anti-parallel diodes (D_1–D_4) respectively.

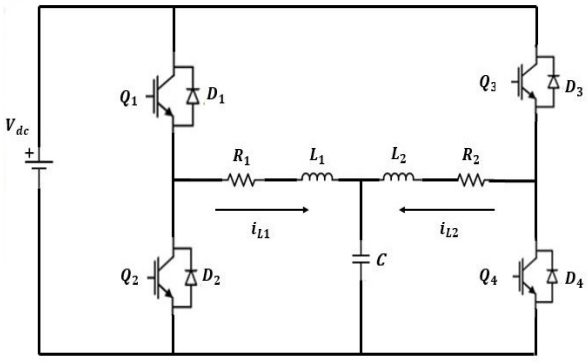

Fig. 1 – Dual-output half-bridge resonant inverter based induction cooker.

Each diode provides the path for conduction of the load current for free-wheeling operation. Both half-bridge inverters convert the input dc voltage V_{dc} to very high frequency ac voltage. The impedance of each any series resonant load can be expressed as

$$Z = R + \mathrm{j}X = R + \mathrm{j}\left(\omega_{sw}L - \frac{1}{\omega_{sw}C}\right) = R\left[1 + \mathrm{j}Q_l\left(\omega_{nsw} - \frac{1}{\omega_{nsw}}\right)\right]. \quad (1)$$

The magnitude and the phase angle are expressed by the following equations.

$$|Z| = R\sqrt{1 + Q_l^2\left(\omega_{nsw} - \frac{1}{\omega_{nsw}}\right)^2}, \quad (2)$$

$$\phi = \tan^{-1}\left\{Q_l\left(\omega_{nsw} - \frac{1}{\omega_{nsw}}\right)\right\}, \quad (3)$$

where

$$\omega_{nsw} = \frac{\omega_{sw}}{\omega_{or}}. \quad (4)$$

is selected as the normalized switching frequency;

[1] Indian Institute of Technology (Indian School of Mines), Research Scholar in Electrical Engineering Department, Dhanbad, 826004, Jharkhand, India, E-mail: ab.chakt@gmail.com
[2] Indian Institute of Technology (Indian School of Mines), Electrical Engineering Department, Dhanbad - 826004, Jharkhand, India
[3] IBM India Private Limited, India
[4] Saroj Mohan Institute of Technology, Guptipara, Hooghly-712512, West Bengal, India

$$\omega_{or} = \frac{1}{\sqrt{LC}} \tag{5}$$

is the resonant angular frequency in rad/s; $\omega_{sw} = 2\pi f_{sw}$ is the angular switching frequency in rad/s; f_{sw} is the IGBT switching frequency in Hertz and the Quality factor of the load is

$$Q_l = \frac{\omega_{or} L}{R} = \frac{1}{\omega_{or} RC} = \frac{Z_c}{R} \tag{6}$$

The characteristic impedance of the system can be expressed as

$$Z_c = \sqrt{\frac{L}{C}} = \frac{1}{\omega_{or} C} = \omega_{or} L \tag{7}$$

The switching frequencies of the two inverters are same to avoid acoustic noise and are selected above the resonant frequency to achieve zero voltage switching (ZVS) operating conditions.

3. ANALYSIS OF TWO PORT NETWORK MODEL

To understand the analytical behaviour of the proposed induction cooking system, the two-port network model is considered as shown in Fig. 2.

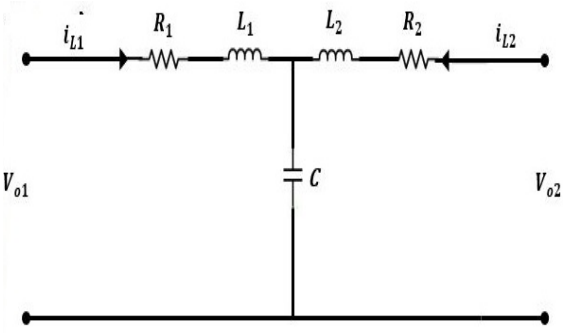

Fig. 2 – Two-port network model of the induction cooker.

In this model, the two inductive loads are assumed to be series RL combinations. The impedances of the two inductive loads can be expressed as:

$$Z_1 = R_1 + \mathrm{j}\omega L_1 \tag{8}$$

$$Z_2 = R_2 + \mathrm{j}\omega L_2 \tag{9}$$

The mutual impedance between the two coils can be represented as:

$$Z_M = R_M + \mathrm{j}\omega L_M \tag{10}$$

The frequency domain representation of the output voltages can be expressed according to the two-port network model.

$$\begin{bmatrix} V_{o1}(\omega) \\ V_{o2}(\omega) \end{bmatrix} = \begin{bmatrix} Z_1(\omega)+Z_c(\omega) & Z_M(\omega)+Z_c(\omega) \\ Z_M(\omega)+Z_c(\omega) & Z_2(\omega)+Z_c(\omega) \end{bmatrix} \begin{bmatrix} i_{L1}(\omega) \\ i_{L2}(\omega) \end{bmatrix}, \tag{11}$$

$$\begin{bmatrix} V_{o1}(\omega) \\ V_{o2}(\omega) \end{bmatrix} = \begin{bmatrix} Z_{11}(\omega) & Z_{12}(\omega) \\ Z_{21}(\omega) & Z_{22}(\omega) \end{bmatrix} \begin{bmatrix} i_{L1}(\omega) \\ i_{L2}(\omega) \end{bmatrix}, \tag{12}$$

where capacitive reactance is expressed as follows

$$Z_c = \frac{1}{\mathrm{j}\omega C}, \tag{13}$$

$$Z_{11}(\omega) = Z_1(\omega) + Z_c(\omega), \tag{14}$$

$$Z_{22}(\omega) = Z_1(\omega) + Z_c(\omega), \tag{15}$$

$$Z_{12}(\omega) = Z_{21}(\omega) = Z_M(\omega) + Z_c(\omega). \tag{16}$$

4. ANALYSIS OF ASYMMETRICAL DUTY CYCLE PHASE-SHIFT CONTROL SCHEME

The output powers of the proposed dual output induction cooking system are controlled by the asymmetrical duty cycle phase-shift control technique. The simplified equivalent circuit of the proposed induction cooker is shown in Fig. 3.

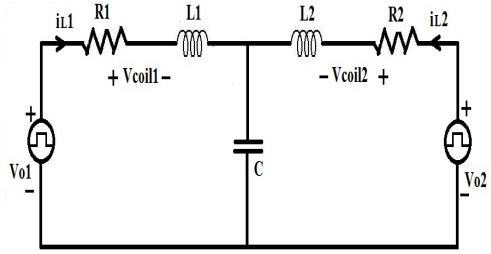

Fig. 3 – Simplified equivalent circuit of the induction cooker.

The output voltages of the dual half-bridge series resonant inverters with asymmetrical duty cycle phase-shift control can be expressed in terms of Fourier series as given below.

$$V_{o1}(t) = \sum_{m=-\infty}^{\infty} a_{m1} \mathrm{e}^{\mathrm{j}m\omega_{sw}t} \tag{17}$$

$$V_{o2}(t) = \sum_{m=-\infty}^{\infty} a_{m2} \mathrm{e}^{\mathrm{j}m\omega_{sw}t} \mathrm{e}^{-\mathrm{j}m\omega_{sw}t_D}, \tag{18}$$

where

$$a_{m1} = \frac{V_{dc}}{\pi m}\left[1 - \mathrm{e}^{-\mathrm{j}m\omega_{sw}D_1T_{sw}}\right] \tag{19}$$

$$a_{m2} = \frac{V_{dc}}{\pi m}\left[1 - \mathrm{e}^{-\mathrm{j}m\omega_{sw}D_2T_{sw}}\right] \tag{20}$$

for $m = 1, 3, 5, \ldots$etc.

Moreover, $\omega_{sw} = \dfrac{2\pi}{T_{sw}}$, $t_D =$ time delay or phase-shift between the output voltages of the dual inverters; $T_{sw} =$ time-period of the switching cycle; D_1 and D_2 are the duty cycles of the two inverters. Phase-shift angle $\phi = \omega_{sw} t_D$.

The output current can be expressed as:

$$[I_L(\omega)] = [Y(\omega)][V_o(\omega)], \tag{21}$$

$$\begin{bmatrix} i_{L1}(\omega) \\ i_{L2}(\omega) \end{bmatrix} = \begin{bmatrix} Y_{11}(\omega) & Y_{12}(\omega) \\ Y_{21}(\omega) & Y_{22}(\omega) \end{bmatrix} \begin{bmatrix} V_{o1}(\omega) \\ V_{o2}(\omega) \end{bmatrix}, \tag{22}$$

where

$$Y_{11} = \frac{Z_{22}}{\Delta Z} = \frac{Z_2 + Z_c}{\left(1-k^2\right)Z_1Z_2 + Z_c\left(Z_1 + Z_2 - 2k\sqrt{Z_1Z_2}\right)} \tag{23}$$

$$Y_{22}=\frac{Z_{11}}{\Delta Z}=\frac{Z_1+Z_c}{\left(1-k^2\right)Z_1Z_2+Z_c\left(Z_1+Z_2-2k\sqrt{Z_1Z_2}\right)} \quad (24)$$

$$Y_{12}=-\frac{Z_{12}}{\Delta Z}=-\frac{Z_M+Z_c}{\left(1-k^2\right)Z_1Z_2+Z_c\left(Z_1+Z_2-2k\sqrt{Z_1Z_2}\right)} \quad (25)$$

$$Y_{21}=-\frac{Z_{21}}{\Delta Z}=-\frac{Z_M+Z_c}{\left(1-k^2\right)Z_1Z_2+Z_c\left(Z_1+Z_2-2k\sqrt{Z_1Z_2}\right)} \quad (26)$$

$$Z_M=k\sqrt{Z_1Z_2} \quad (27)$$

$$\Delta Z=Z_{11}Z_{22}-Z_{12}Z_{21}. \quad (28)$$

From Equation (22), it is revealed that the output current through each load has two components. The first component is due to the current generated by each inverter involving the coefficient of coupling k which is expressed by following equations:

$$i_{L1r}=Y_{11}V_{o1}=$$
$$=\sum_{m=-\infty}^{\infty}\frac{a_{m1}\left(Z_2+Z_c\right)\mathrm{e}^{\mathrm{j}m\omega_{sw}t}}{\left(1-k^2\right)Z_1Z_2+Z_c\left(Z_1+Z_2-2k\sqrt{Z_1Z_2}\right)} \quad (29)$$

$$i_{L2r}=Y_{22}V_{o2}=$$
$$=\sum_{m=-\infty}^{\infty}\frac{a_{m2}\left(Z_1+Z_c\right)\mathrm{e}^{\mathrm{j}m\omega_{sw}(t-t_D)}}{\left(1-k^2\right)Z_1Z_2+Z_c\left(Z_1+Z_2-2k\sqrt{Z_1Z_2}\right)}. \quad (30)$$

The first component is also related to the diagonal elements of the admittance matrix $Y(\omega)$. The first current components are current driven by each coil connected to the harmonic voltage sources. Equation (22) also includes the second component of the output current through each load that can be expressed as:

$$i_{L1s}=Y_{12}V_{o2}=$$
$$=\sum_{m=-\infty}^{\infty}-\frac{a_{m2}\left(Z_M+Z_c\right)\mathrm{e}^{\mathrm{j}m\omega_{sw}(t-t_D)}}{\left(1-k^2\right)Z_1Z_2+Z_c\left(Z_1+Z_2-2k\sqrt{Z_1Z_2}\right)} \quad (31)$$

$$i_{L2s}=Y_{21}V_{o1}=$$
$$=\sum_{m=-\infty}^{\infty}-\frac{a_{m1}\left(Z_M+Z_c\right)\mathrm{e}^{\mathrm{j}m\omega_{sw}t}}{\left(1-k^2\right)Z_1Z_2+Z_c\left(Z_1+Z_2-2k\sqrt{Z_1Z_2}\right)}. \quad (32)$$

The second components are related to the non-diagonal elements of the admittance matrix $Y(\omega)$. The second current components are driven by the opposite inductor coil. Then the total output current through load1 can be expressed by the following equation.

$$i_{L1}(\omega)=i_{L1r}(\omega)+i_{L1s}(\omega) \quad (33)$$

where $i_{L1r}(\omega)$ is the current driven by the coil1fed by harmonic voltage source $V_{o1}(m\omega_{sw})$ and $i_{L1s}(\omega)$ is the current driven by the coil1 fed by the harmonic voltage source $V_{o2}(m\omega_{sw})$. Similarly, the total output current through load2 can be expressed by the following equation.

$$i_{L2}(\omega)=i_{L2r}(\omega)+i_{L2s}(\omega), \quad (34)$$

where $i_{L2r}(\omega)$ is the current driven by the coil2 fed by harmonic voltage source $V_{o2}(m\omega_{sw})$ and $i_{L2s}(\omega)$ is the current driven by the coil2 fed by the harmonic voltage source $V_{o1}(m\omega_{sw})$.

Now, if $V_{coil1}(t)$ and $V_{coil2}(t)$ be the voltages across coil1 and coil2 respectively, then they can be expressed by the following equations

$$V_{coil1}(t)=V_{coil1r}(t)+V_{coil1s}(t) \quad (35)$$

$$V_{coil2}(t)=V_{coil2r}(t)+V_{coil2s}(t), \quad (36)$$

where:

$$V_{coil1r}(t)=\sum_{m=-\infty}^{\infty}Z_1(m\omega_{sw})Y_{11}(m\omega_{sw})V_{o1}(m\omega_{sw}) \quad (37)$$

$$V_{coil1s}(t)=\sum_{m=-\infty}^{\infty}Z_1(m\omega_{sw})Y_{12}(m\omega_{sw})V_{o2}(m\omega_{sw}) \quad (38)$$

$$V_{coil2r}(t)=\sum_{m=-\infty}^{\infty}Z_2(m\omega_{sw})Y_{22}(m\omega_{sw})V_{o2}(m\omega_{sw}) \quad (39)$$

$$V_{coil2s}(t)=\sum_{m=-\infty}^{\infty}Z_2(m\omega_{sw})Y_{21}(m\omega_{sw})V_{o1}(m\omega_{sw}). \quad (40)$$

The power generated in coil1 can be obtained by the following equation

$$P_1=<V_{coil1}(t)i_{L1}(t)>_{T_{sw}}=$$
$$=<V_{coil1r}(t)i_{L1r}(t)>_{T_{sw}}+<V_{coil1r}(t)i_{L1s}(t)>_{T_{sw}} \quad (41)$$
$$+<V_{coil1s}(t)i_{L1r}(t)>_{T_{sw}}+<V_{coil1s}(t)i_{L1s}(t)>_{T_{sw}}.$$

The first and the fourth terms of the above equation are associated with the dissipating power in the coil1, which does not depend on the phase-shift between the two inverters.

On the other hand, the second and the third terms are associated with the inter-coupled power between the two partly magnetically coupled coils, which depends on the phase-shift between the two inverters.

Hence, dissipating power in the coil1 is expressed as follows

$$P_{1d}=<V_{coil1r}(t)i_{L1r}(t)>_{T_{sw}}+<V_{coil1s}(t)i_{L1s}(t)>_{T_{sw}}=$$
$$=\sum_{m=1,3,5,..}^{\infty}R_1\left|Y_{11}(m\omega_{sw})\right|^2\left|V_{o1}(m\omega_{sw})\right|^2+ \quad (42)$$
$$+R_1\left|Y_{12}(\omega_{sw})\right|^2\left|V_{o2}(\omega_{sw})\right|^2.$$

Moreover, the inter-coupled power in coil1 can be expressed as follows.

$$P_{1c}=<V_{coil1r}(t)i_{L1s}(t)>_{T_{sw}}+<V_{coil1s}(t)i_{L1r}(t)>_{T_{sw}}=$$
$$=R_1Y_{11}(\omega_{sw})Y_{12}^*(\omega_{sw})V_{o1}(\omega_{sw})V_{o2}^*(\omega_{sw})+ \quad (43)$$
$$+R_1Y_{12}(\omega_{sw})Y_{11}^*(\omega_{sw})V_{o2}(\omega_{sw})V_{o1}^*(\omega_{sw}),$$

hence

$$P_1=P_{1d}+P_{1c}. \quad (44)$$

Similarly, the power generated in coil2 can be expressed as follows

$$P_2 = < V_{coil2}(t) i_{L2}(t) >_{T_{sw}} = \\ = < V_{coil2r}(t) i_{L2r}(t) >_{T_{sw}} + < V_{coil2r}(t) i_{L2s}(t) >_{T_{sw}} + \\ + < V_{coil2s}(t) i_{L2r}(t) >_{T_{sw}} + < V_{coil2s}(t) i_{L2s}(t) >_{T_{sw}} . \quad (45)$$

The dissipating power in coil2 can be expressed as

$$P_{2d} = \\ = < V_{coil2r}(t) i_{L2r}(t) >_{T_{sw}} + < V_{coil2s}(t) i_{L2s}(t) >_{T_{sw}} \\ = \sum_{m=1,3,5,..}^{\infty} R_2 |Y_{22}(m\omega_{sw})|^2 |V_{o2}(m\omega_{sw})|^2 + \quad (46) \\ + R_2 |Y_{21}(\omega_{sw})|^2 |V_{o1}(\omega_{sw})|^2 .$$

Here, P_{2d} does not depend on the phase-shift between the two inverters.

Similarly, the inter-coupled power in coil2 can be expressed as follows.

$$P_{2c} = < V_{coil2r}(t) i_{L2s}(t) >_{T_{sw}} + < V_{coil2s}(t) i_{L2r}(t) >_{T_{sw}} = \\ = R_2 Y_{22}(\omega_{sw}) Y_{21}^*(\omega_{sw}) V_{o2}(\omega_{sw}) V_{o1}^*(\omega_{sw}) + \quad (47) \\ + R_2 Y_{21}(\omega_{sw}) Y_{22}^*(\omega_{sw}) V_{o1}(\omega_{sw}) V_{o2}^*(\omega_{sw}).$$

Here, P_{2c} depends on the phase-shift between the two inverters.

Hence,

$$P_2 = P_{2d} + P_{2c} . \quad (48)$$

Since, the common resonance capacitor offers almost zero impedance path for high frequency current components other than the fundamental, so, the second current component term of both P_{1d} and P_{2d} only consists of the fundamental component. Similarly, the inter-coupled powers P_{1c} and P_{2c} also carry the fundamental component only. Besides, the dissipating powers P_{1d} and P_{2d} in both the coils do not depend on the phase-shift angle ϕ between the inverters but depend on the duty cycles D_1, D_2 and the angular switching frequency ω_{sw} respectively. On the other hand, the inter-coupled power P_{1c} and P_{2c} depend significantly on the on the phase-shift angle ϕ between the inverters and as well as on the duty cycles D_1, D_2 and the angular switching frequency ω_{sw} respectively.

5. REAL-TIME HARDWARE EXPERIMENT

To verify the proposed two-port network model, a real-time experimental setup is implemented as shown in Fig. 4. The proposed model has two half-bridge resonant inverters operating with a switching frequency of 38.5 kHz and connected to a 230 V dc source V_{dc}. The equivalent parameters of the two induction heating loads are $R_1 = 5\Omega$, $L_1 = 35$ μH, $R_2 = 4$ Ω and $L_2 = 28$ μH. Furthermore, the value of the common resonant capacitor is $C = 1.39$ μF.

Fig. 4 – Real time hardware experimental setup.

6. VERIFICATION OF SIMULATION RESULTS WITH EXPERIMENTAL RESULTS

To understand the performance of the asymmetrical duty cycle phase-shift control of the proposed dual output induction cooker, PSIM simulation is carried out. The results obtained from the PSIM simulation are shown in Fig. 5, Fig. 6, Fig. 7 and Fig. 8 respectively. From Fig. 5 and Fig. 6, it is clear that the currents driven by both coil1 and coil2 are sinusoidal in nature with a phase-shift angle $\phi = 60^\circ$, which means that for low phase-shift angle the current carried by each coil although consists of two current components, but the second current component due to the phase-shift is very less with respect to the current through each coil contributed by individual inverter operations. On the other hand, in Fig. 7 and Fig. 8, distortions occur in the currents through both the coils at large phase-shift angle $\phi = 240^\circ$, signifies that current component contributed due to the phase-shift is relatively large compared to the current components by the inverter operations. Moreover, Fig. 9 and Fig. 10 are presenting the current waveforms in the oscilloscope through each coil obtained from the real-time hardware experiments for $D_1 = 0.3$, $D_2 = 0.4$. These waveforms match with the waveforms obtained from the simulation. Nevertheless, Fig. 11 and Fig. 12 show the variation of the generated powers in the coil1 and coil2 with respect to the phase-shift angle ϕ involving both simulation results and hardware experimental results. It is found that the simulated and hardware experimental results are totally matched for $D_1 = 0.3$, $D_2 = 0.4$ and $D_1 = 0.53$, $D_2 = 0.3$ respectively.

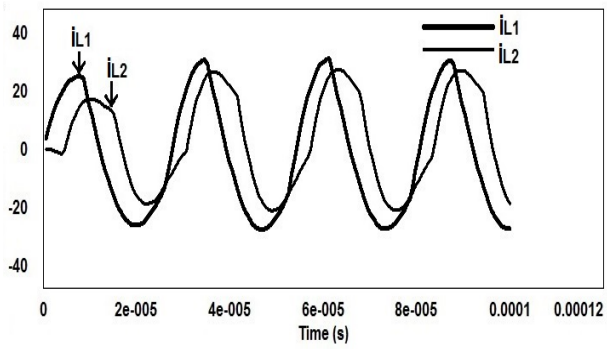

Fig. 5 – Currents driven by coil1 i_{L1} (thick line) and coil2 i_{L2} (thin line) with a phase-shift of 60 degrees at a switching frequency of 38.5 kHz with $D_1 = 0.3$ and $D_2 = 0.4$.

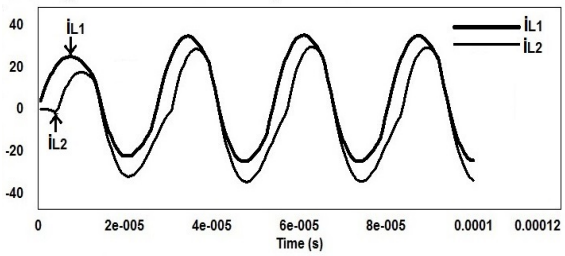

Fig. 6 – Currents driven by coil1 i_{L1} (thick line) and coil2 i_{L2} (thin line) with a phase-shift of 60 degrees at a switching frequency of 38.5 kHz with $D_1 = 0.5$ and $D_2 = 0.3$.

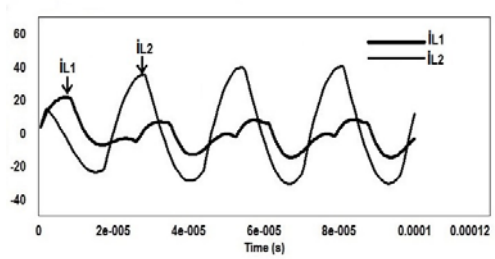

Fig. 7 – Currents driven by coil1 i_{L1} (thick line) and coil2 i_{L2} (thin line) with a phase-shift of 240 degrees at a switching frequency of 38.5 kHz with D_1=0.3 and D_2=0.4.

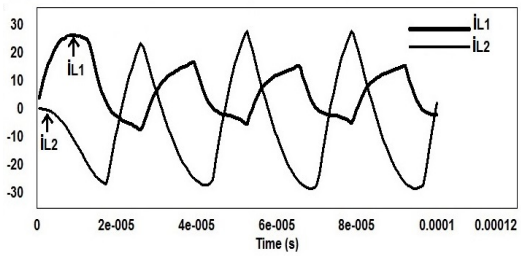

Fig. 8 – Currents driven by coil1 i_{L1} (thick line) and coil2 i_{L2} (thin line) with a phase-shift of 60 degrees at a switching frequency of 38.5 kHz with $D_1 = 0.5$ and $D_2 = 0.3$.

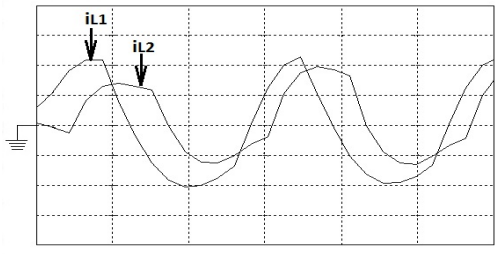

Fig. 9 – Currents of coil1 i_{L1} and coil2 i_{L2} with a phase-shift of 60 degrees at a switching frequency of 38.5 kHz with $D_1 = 0.3$ and $D_2 = 0.4$ from hardware experiment [Y-axis (current): 10 A/div, X-axis (time): 10 μs/div].

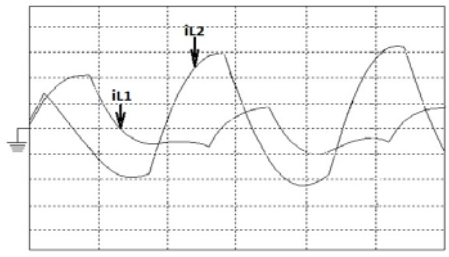

Fig. 10 – Currents of coil1 i_{L1} and coil2 i_{L2} with a phase-shift of 240 degrees at a switching frequency of 38.5 kHz with D_1= 0.3 and D_2=0.4 from hardware experiment [Y-axis (current): 10 A/div, X-axis: 10 μs/div].

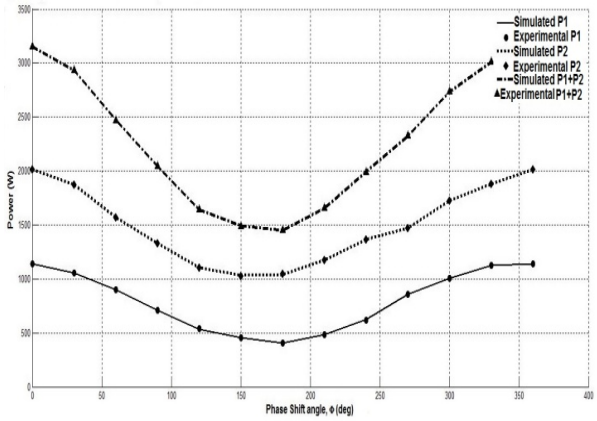

Fig. 11 – Power delivered to two inductive loads with respect to the phase-shift angle ϕ for $D_1 = 0.3$ and $D_2 = 0.4$ from simulated and hardware experimental results.

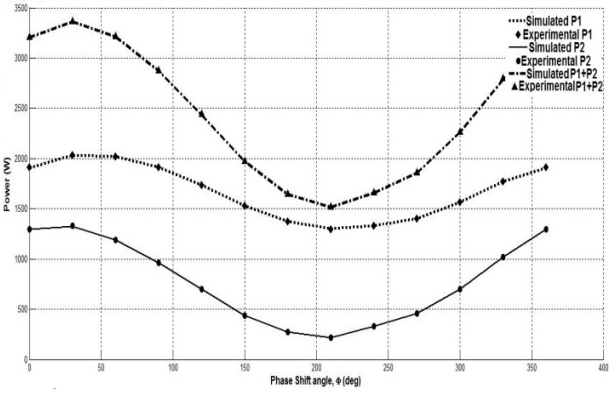

Fig. 12 – Power delivered to two inductive loads with respect to the phase-shift angle ϕ for $D_1 = 0.5$ and $D_2 = 0.3$ from simulated and hardware experimental results.

7. CONCLUSIONS

In this paper, an analytical approach has been made on a dual output induction cooker controlled by asymmetrical duty cycle phase-shift control technique. The proposed model shows a significant matching between the mathematical analysis and the real-time hardware experimental results. So, it can be concluded that the asymmetrical duty cycle phase-shift control is a suitable and effective control technique to control the output power of any advanced multi-output induction cooking systems.

ACKNOWLEDGEMENTS

Authors are thankful to the University Grants Commission, Bahadurshah Zafar Marg,New Delhi, India for granting financial support under Major Research Project entitled “Simulation of high frequency mirror inverter for energy efficient induction heated cooking oven using PSPICE” and also grateful to the Under Secretary and Joint Secretary of UGC, India for their active co-operation.

Received on January 21, 2017

REFERENCES

1. O. Lucía, P. Maussion, E.J. Dede, J.M. Burdío, *Induction Heating Technology and Its Applications: Past Developments, Current Technology,and Future Challenges*, IEEE Transactions on Industrial Electronics, **61**, 5 (2014).
2. A. Chakraborty, P.K. Sadhu, K. Bhaumik, P. Pal, N. Pal, *Behaviour of a High Frequency Parallel Quasi Resonant Inverter Fitted Induction Heater with Different Switching Frequencies*, International Journal of Electrical and Computer Engineering, **6**, *2*, pp. 447–457 (2016).
3. Y.S. Kwon, S.B. Yoo, D.S. Hyun*, Half: Bridge series resonant inverter for induction heating applications with load adaptive PFM control strategy*, Proc. IEEE Power Electronics Conference and Exposition (APEC), **I**, pp. 575–581 (1999).
4. V. Esteve, J. Jordán, E.S. Kilders, E.J. Dede, M.E. Maset, J.B. Ejea, A. Ferreres*, Improving the Reliability of Series Resonant Inverters for Induction Heating Applications*, IEEE Transactions on Industrial Electronics, **61**, 5 (2014).
5. V.V.S.K. Bhajana, P. Drabek, M. Jara, *Performance Evaluation of LLC Resonant Full Bridge DC-DC Converter for Auxiliary Systems in Traction*, Rev. Roum. Sci. Techn. – Électrotechn. et Énerg., **60**, *1*, pp. 79–88 (2015).
6. A. Bhattacharya, P.K. Sadhu, A. Bhattacharya, N. Pal, *Voltage Controlled Resonant Inverter – An Essential Tool For Induction Heated* Equipment, Rev. Roum. Sci. Techn. – Électrotechn. et Énerg., **61**, *3*, pp. 273–277 (2016).
7. B.Y. Chenand, Y.S. Lai, *Switching Control Technique of Phase-Shift-Controlled Full-Bridge Converter to Improve Efficiency under Light-Load and Standby Conditions without Additional Auxiliary Components*, IEEE Transactions on Power Electronics, **25**, *4* (2010).
8. S.H. Hosseini, A.Y. Goharrizi, E. Karimi, *A multioutput series resonant inverter with asymmetrical voltage-cancellation control for induction-heating cooking appliances*, Proc. IEEE Power Electronics and Motion Control Conference(IPEMC), **3**, pp. 1–6 (2006).
9. Vicente Esteve, Esteban Sanchis-Kilder, José Jordán , Enrique J. Dede, César Cases, Enrique Maset , Juan B. Ejea, Agustín Ferreres, *Improving the Efficiency of IGBT Series-Resonant Inverters Using Pulse Density Modulation*, IEEE Transactions on Industrial Electronics, **58**, *3* (2011).
10. T. Leuca, Ş. Nagy, N.D. Trip, Helga Silaghi, Claudiu Mich-Vancea, *Optimal Design for Induction Heating using Genetic algorithms*, Rev. Roum. Sci. Techn. – Électrotechn. et Énerg., **60**, *2*, pp. 133–142 (2015).